

Article

Not peer-reviewed version

# CT-Based Radiomics to Predict the KRAS Mutation in CRC patients. A Retrospective Study.

[Jacobo Porto Álvarez](#)\*, [Eva Cernadas](#)\*, Rebeca Aldaz Martínez, [Manuel Fernández-Delgado](#), Emilio Huelga Zapico, [Victor González-Castro](#), [Sandra Baleato González](#)\*, Roberto Garcia-Figueiras, J Ramon Antunez-Lopez, [Miguel Souto-Bayarri](#)

Posted Date: 30 June 2023

doi: 10.20944/preprints202306.2239.v1

Keywords: KRAS mutation; colorectal cancer; texture analysis; radiomics, radiogenomics.



Preprints.org is a free multidiscipline platform providing preprint service that is dedicated to making early versions of research outputs permanently available and citable. Preprints posted at Preprints.org appear in Web of Science, Crossref, Google Scholar, Scilit, Europe PMC.

Copyright: This is an open access article distributed under the Creative Commons Attribution License which permits unrestricted use, distribution, and reproduction in any medium, provided the original work is properly cited.

## Article

# CT-Based Radiomics to Predict the KRAS Mutation in CRC patients. A Retrospective Study.

Jacobo Porto-Álvarez <sup>1</sup>, Eva Cernadas <sup>3</sup>, Rebeca Aldaz Martínez <sup>1</sup>, Manuel Fernández-Delgado <sup>3</sup>, Emilio Huelga Zapico <sup>1</sup>, Víctor González-Castro <sup>2</sup>, Sandra Baleato González <sup>1</sup>, Roberto García Figueiras <sup>1</sup>, Antúnez-López José Ramón <sup>4</sup> and Miguel Souto-Bayarri <sup>1</sup>

<sup>1</sup> Department of Radiology, Complejo Hospitalario Universitario de Santiago de Compostela, 15706 Santiago de Compostela, Spain.

<sup>2</sup> Department of Electrical, Systems and Automation Engineering, Universidad de León, Campus de Vegazana s/n, 24071 León, Spain.

<sup>3</sup> Centro Singular de Investigación en Tecnoloxías Intelixentes da USC (CITIUS), Universidade de Santiago de Compostela, Spain.

<sup>4</sup> Department of Pathology, Complejo Hospitalario Universitario de Santiago, USC, 15706 Santiago de Compostela, Spain.

\* Correspondence: eva.cernadas@usc.es (ECG), Sandra.baleato.gonzalez@sergas.es (S.B.G.), jacoboporto.alvarez2@sergas.es (J.P.A.)

**Abstract:** Colorectal cancer (CRC) is one of the most common types of cancer worldwide. The KRAS mutation is present in 30-50% of CRC patients. This mutation confers resistance to treatment with anti-EGFR therapy. This article aims at proving that Computer Tomography (CT)-based Radiomics can predict the KRAS mutation in CRC patients. The piece is a retrospective study with 56 CRC patients from the Hospital of Santiago de Compostela, Spain. All patients had a confirmatory pathological analysis of the KRAS status. Radiomics features were obtained from the abdominal contrast enhancement CT (CECT), before applying any treatments. We used several classifiers, including adaboost, neural network, decision tree, support vector machine and random forest, to predict the presence or absence of KRAS mutation. The most reliable prediction was achieved using the adaboost ensemble on clinical patient data, with a kappa and accuracy of 53.7% and 76.8%, respectively. The sensitivity and specificity were of 73.3% and 80.8%. Using texture descriptors, the best accuracy and kappa were 73.2% and 46%, respectively, with sensitivity and specificity of 76.7% and 69.2%, showing also a correlation between texture patterns on CT images and KRAS mutation. Radiomics could help manage CRC patients, and in the future, it could have a crucial role in diagnosing CRC patients ahead of invasive methods.

**Keywords:** KRAS mutation; colorectal cancer; texture analysis; radiomics; radiogenomics

## 1 Introduction

The carcinogenesis of colorectal cancer is a heterogeneous process encompassing a series of genetic, epigenetic and molecular changes in the cells that line the colonic mucosa [1,2]. These changes are influenced by dietary, environmental, and microbiotic factors and the host's immune response [3,4]. The successive activation of oncogenes (KRAS, NRAS, BRAF, PIK3CA, ERBB2) while inactivating tumour suppressor genes (APC, TP53, PTEN, TGF- $\beta$ , DCC) guides the adenoma-carcinoma transition [5,6]. KRAS is a gene of the RAS/MAPK pathway. RAS proteins are a family of proteins expressed in all cells within the intracellular cascade associated with tyrosine-kinase receptors. This pathway stimulates cell proliferation, differentiation, adhesion, apoptosis and migration [7]. Up to 60-80% of colorectal cancers overexpress EGFR (Epidermal Growth Factor Receptors), which are tyrosine-kinase receptors, and this is an important component in the initiation and

progression of colorectal cancer [8,9]. The anti-EGFR antibodies (cetuximab or panitumumab) has a therapeutic effect in patients with colorectal cancer. When there is a mutation in this pathway, such as KRAS mutation, these therapies cannot be employed because it confers resistance to EGFR antibodies. The KRAS mutation is present in 30-50% of colorectal cancers [9], and this mutation is associated with worse survival, so it is considered as a negative prognostic factor [10,11].

Radiomics is the transformation of radiological images into structured data that can be used to support decision making in day-to-day clinical practice. Data that are not visible to the human eye are taken into account through radiomic analysis of a radiological image [12,13]. The development of radiomics has been more pronounced in the field of oncology. There are several studies published in recent years using radiomics in different cancers and using different imaging modalities, such as magnetic resonance imaging (MRI), ultrasound and CT [14].

This article aims to predict the presence of KRAS mutation in colorectal cancer patients using a CT-based radiomics model. To achieve this goal, it is necessary to extract the radiomics features from the CT images and automatically classify the patients as KRAS + or KRAS- using machine learning algorithms belonging to different classifiers families, such as support vector machine, neural network, linear discriminant analysis, decision trees and ensembles, among others. A second objective of this article is to explore the performance of clinical data and whether it can improve the radiomic model when both are combined. To this purpose, data such as tumour location, presence of hepatic or pulmonary metastases, as well as tumour stage and differentiation are included. The results were compared with the anatomopathological analysis of the tumour using Cohen's Kappa statistic, sensitivity and specificity.

Anatomopathological analysis of the tumour is the gold standard for determining KRAS mutation, but it is an invasive test, and it only analyses a portion of the tumour. Radiomics is a non-invasive method that can help determine KRAS status by localizing the area of the tumour most likely to have a KRAS mutation and guiding the biopsy.

## 2. Materials and Methods

### 2.1. Radiomics workflow

Radiomics workflow consists of five sequential steps: image acquisition, pre-processing, region of interest segmentation, feature extraction and analysis [Figure 1][13,14].

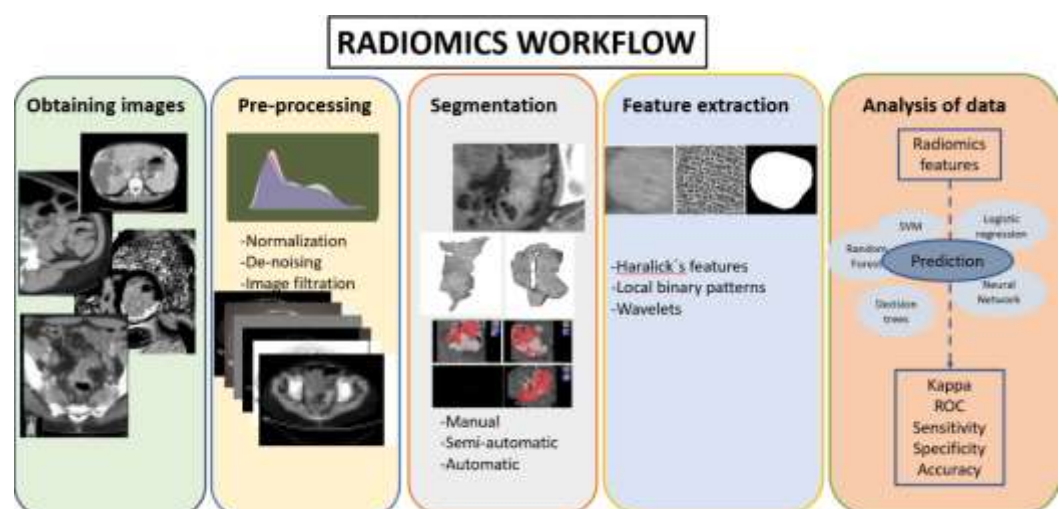


**Figure 1.** Radiomics workflow.

### 2.2. Patient selection and obtaining imaging

For this retrospective study, 56 patients from the Santiago de Compostela Health District were selected. The inclusion criteria were defined as follows: (1) colorectal cancer

patients with anatomopathological confirmation of KRAS status by biopsy between 2016 and 2019 (30 KRAS+ and 26 KRAS- patients, respectively); (2) intravenous CECT performed before any treatment; (3) CT images with a slice thickness of less than 5 mm. The exclusion criteria were as follows: (1) patients with colorectal cancer in which the anatomopathological analysis was performed after any type of treatment; (2) CT with a slice thickness other than that specified; (3) patients with a tumour difficult to delineate. The conduct of this research has been approved by the Ethics Committee.

### 2.3. Segmentation

The segmentation performed was a manual segmentation by an expert abdominal radiologist. The software used for the segmentation was Sectra IDS7 visualization program, which is the software used by the radiology department of the Clinic Hospital of Santiago de Compostela.

Three slices of the tumour were selected, the slice with the largest tumour area (central slice), and the slices immediately cranial and caudal to that central slice. For each slice, 4 images were obtained, 2 of them with the tumour manually segmented. A total of 12 images were obtained for each patient. The images were saved in ".tiff" format.

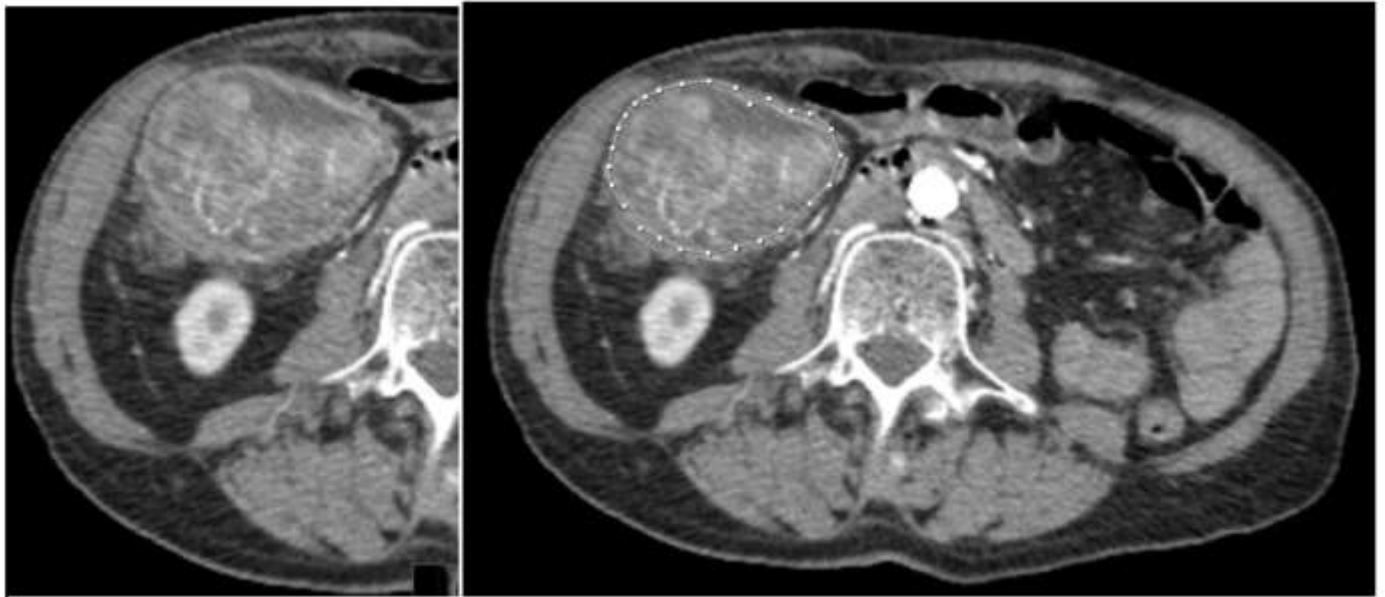


**Figure 2.** 58-year-old patient with KRAS mutated CRC. a) Tumour without any segmentation. b) Tumour manually segmented by an expert abdominal radiologist.



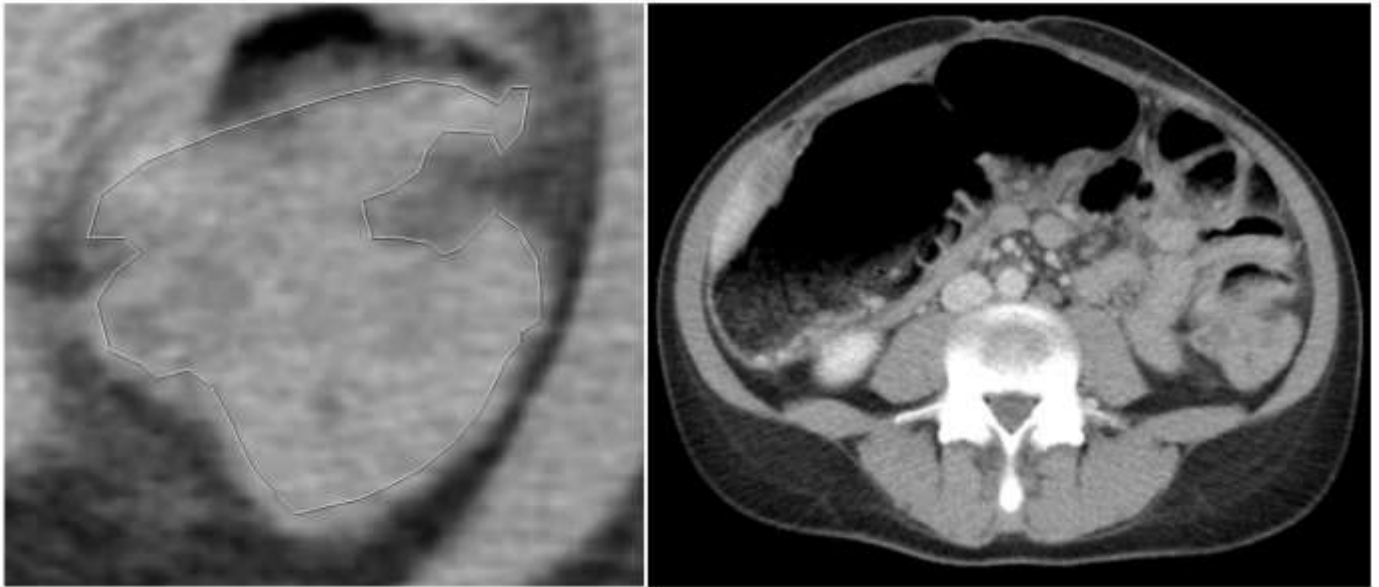


**Figure 3.** a) Manually segmented non-mutated KRAS tumour. b) Abdominal contrast-enhancement CT of the same patient.

#### 2.4. Pre-processing and Feature extraction

The texture is a visual image property related to the spatial distribution of grey level of pixels [15], which may be used for image classification. The feature extraction algorithms transform an image or region of interest (ROI) in the image into a feature vector, which will be used to do the classification. Some of the techniques provided in the literature can only be applied to rectangular or even squared regions [16], and they are not suitable for our problem, in which the cancer tumors are irregular regions. In previous works, some popular texture extraction techniques were adapted to operate over irregular ROIs [19,21]. For example, the frequency techniques, like Gabor or Fourier filters, are global techniques and cannot be adapted to operate on irregular regions. Among the statistical techniques, we use in this study the Haralick coefficients and the local binary patterns (LBP), which are described in our previous work [19]. Let  $G=\{0, 1, \dots, N_g-1\}$  the number of grey levels,  $S$  a finite set of pixels specifying the region of interest (ROI) to be analysed (in our case, the tumour),  $I(x,y) \in G$  the grey level in the pixel  $(x,y) \in S$ . To compute Haralick coefficients [17], the grey level cooccurrence matrix,  $M$ , count the occurrence of pixel  $(x_i, y_i) \in S$  and  $(x_j, y_j) \in S$  with a grey level  $g_i$  and  $g_j \in G$  in a specific orientation  $\theta$  and scale, i.e. different distance,  $d=\{1,2,3\}$ , from one pixel to each other. The matrices  $M$ , of dimension  $N_g \times N_g$ , are calculated for different orientations and scales. Normally, the matrices  $M$  for different orientations are averaged in order to achieve rotation invariance. The energy, correlation, contrast, homogeneity and entropy are derived from the matrix  $M$  for each scale. Eight Haralick vectors  $Hf_{dm}$  are calculated varying the distance  $d$ , to be  $d=\{1, 2, 3\}$  pixels, alongside with another vector concatenating the previous three distances,  $d=123$ , and the number of Haralick coefficients  $m=\{4, 5\}$  depending of entropy coefficient is included or not:  $\{Hf_{dm}, d=1, 2, 3, 123, m=4, 5\}$ .

The local binary patterns (LBP) [20] algorithm extracts the dependence of pixels in a neighborhood comparing the grey level of central pixel with the surrounding ones. Among the variants proposed in the literature, we use the LBP uniform patterns, i.e. patterns which a limited number of transitions from 0 to 1 or vice versa, lower, or equal than two. Four texture feature vectors, called  $LBP_R$ , one for each radius  $R=\{1,2,3\}$  using a neighborhood of  $P=8$  pixels. The  $LBP_R$  contains 10 features for each scale or radius, representing a histogram of the number of transitions in the pixels  $(x,y) \in S$ . The feature vector  $LBP_{123}$  with 30 features for the concatenation of the previous three  $LBP_R$  vectors:  $\{LBP_R, R=1, 2, 3, 123\}$ .

The Discrete Wavelet Transform (DWT) is another very popular spectral technique for texture extraction, which is normally applied on a squared region whose side is a power of 2. A multi-scale decomposition is obtained applying recursively low-pass and high-pass filters and downsampling to the image. Statistical measures over the transform coefficients for each sub-band and decomposition level are normally used to encode texture information. The measured used are mean, energy, entropy, and standard deviation, calculated in the pixels  $(x,y) \in S$ . We compute the vector DWT using three levels of decomposition and calculating the energy, entropy, mean, and standard deviation measures over all subbands developing a vector with 52 features.

We derive texture descriptors from the wavelet decomposition in different ways (see our reference [21] for a detailed description):

1. Applying Haralick coefficients over the different wavelet decomposition levels using a distance  $d=1$ , due to the scale is implicitly included in the downsampling. We compute four vectors, called  $WDCF_{fm}$ , varying the number of Haralick coefficients  $m=\{4,5\}$  and the type of decomposition  $f=\{LL, All\}$  using a distance  $d = 1$ :  $\{WDCF_{fm}, f=LL, All, m=4,5\}$ .
2. Another way to capture multiscale information would be calculating the cooccurrences matrices on the first level of decomposition. We compute the following six vectors ( $WCF_{dm}$ ) varying the distance  $d=\{1,2,3\}$  to calculate the cooccurrences matrices and the number of Haralick's coefficients  $m=\{4,5\}$ :  $\{WCF_{dm}, d=1, 2, 3, m=4, 5\}$ .
3. The multiscale information can also be captured calculating the LBP signature using a radius of one pixel over low-pass wavelet decompositions of the original image. Specifically, the four vectors  $LBP_s$  considering one level of wavelet decomposition  $s=\{1, 2, 3\}$  is computed, developing feature vectors of 10 features. The concatenation of the three previous vectors is called  $LBP_{123}$  with 30 features:  $\{LBP_s, s=1, 2, 3, 123\}$ .

2.5. Machine learning models

Machine Learning is widely used in medicine to predict different indicators. Our attempt is the prediction of KRAS status, in which there are two possible labels, patient with KRAS+ or KRAS-, being the former considered as a “positive event” to be detected. So, this prediction is an case of binary classification. Among the classifiers proposed in the literature, we have selected a reduced number among the best-performing classifiers in our exhaustive comparison [21] from all the classifier families. The classifiers are trained to learn from the input data (texture features and patient clinical information, see below) how to predict the output (KRAS+ or KRAS-). In this training process the classifier uses a collection of examples composed by input data and desired output (gold standard). The trained classifier can predict, with more or less reliability, the genetic disease of unseen patients. In the current experimental work, we use a collection of 34 classifiers implemented in the programming languages Matlab, Octave, Python and R, belonging to the families: support vector machine, neural network, decision tree, bagging, ensemble and linear discriminant analysis, among others. The table 1 list the information about the classifiers used in this work.

**Table 1.** List of classifiers with their implementation language, function and module/package used and values used for hyper-parameter tuning (the notation 1:2:5 means values from 1 to 5 with step 2).

Family	Classifier	Language	Function (module): Hyperparameter tuning (if any)
Discriminant Analysis	lda: linear discriminant analysis	Octave	Function <b>train_sc</b> with option LD2, package NaN
		Matlab	Function <b>fitcdiscr</b>
		Python	Function <b>LinearDiscriminantAnalysis</b> , module sklearn.discriminant_analysis
		R	Function <b>lda</b> , package MASS
	dlda: diagonal LDA	Matlab	Function <b>fitcdiscr</b> , option DiscrimType=diaglinear

Neural Networks	<b>qda</b> : quadratic discriminant analysis	Matlab	Function <b>fitcdiscr</b> , option DiscrimType=pseudoquadratic
	<b>kfd</b> : kernel Fisher discriminant	Python	Function <b>Kfda</b> , package kfda <sup>1</sup>
	<b>mlp</b> : multilayer perceptron	Matlab	Function <b>fitcnet</b> , $n_h=10$ , $h_1=\max(1, \lfloor N/(I+C) \rfloor)$ , $h_0=\max(1, \lfloor h_1/n_h \rfloor)$ , $\Delta=\max(1, (h_1-h_0)/n_h)$ , $h$ (number of hidden neurons)= $h_0:\Delta:h_1$ , $N$ =no. training patterns, $I$ =no. features
		Python	Function <b>MLPClassifier</b> , module sklearn.neural_network, same $h$
	<b>nnet</b> : multilayer perceptron	R	Function <b>nnet</b> , package nnet, same $h$ , weight decay={0, 0.0001, 0.001, 0.01, 0.1}
	<b>neuralnet</b> : multilayer perceptron	R	Function <b>neuralnet</b> , package neuralnet, same $h$
	<b>elm</b> : extreme learning machine	Octave	<i>Ad-hoc</i> implementation, $h$ (hidden neurons): 20 values in $1..\lfloor N/(I+C) \rfloor$
	<b>svm</b>	Octave	LibSVM library <sup>2</sup> , functions <b>svcmtrain/svmpredict</b> , $\lambda$ (regularization)= $2^{-5:2:10}$ , $\gamma$ (RBF spread)= $2^{-15:2:10}$
		Python	Function <b>SVC</b> , module sklearn.svm, same tuning
		R	Function <b>ksvm</b> , module kernlab, same tuning
K-nearest neighbor	<b>knn</b>	Matlab	Function <b>fitcknn</b> , $k$ (no. neighbors)=1:2:15
		R	Function <b>knn</b> , package class, same $k$
Ensembles	<b>adaboost</b>	Matlab	Function <b>fitcensemble</b> , option method=AdaBoostM1, $T$ (no. trees)=10:10:50
		Python	Function <b>AdaboostClassifier</b> , same $T$ , learning rate=0.1:0.1:0.9
	<b>bagging</b>	R	Function <b>fitcensemble</b> , option method=Bag
	<b>rf</b> : random forest	Python	Function <b>RandomForestClassifier</b> , package sklearn.ensemble, $T=5:5:31$ , $F$ (max. features)=3:2: $I$
	<b>gbm</b> : gradient boosting machine	Python	Function <b>GradientBoostingClassifier</b> , package sklearn.ensemble, $T=\{50,100,150,200\}$ , $D$ (max. depth)={1,3,6,9}
	<b>avNNet</b> : committee of neural multilayer perceptrons	R	Function <b>avNNet</b> , package caret, $H=1..9$ and as nnet, decay=0, 0.1, 0.01, 0.001, 0.0001
Regularized linear regression	<b>Lasso</b>	Matlab	Function <b>fitcecoc</b> , option Learners=templateLinear with Learner=svm and Regularization=lasso or ridge, $\lambda$ (regularization)= $2^{-3:0.2:3}$
	<b>Ridge</b>	Matlab	
	<b>sgd</b> : stochastic gradient descent	Python	Function <b>SGDClassifier</b> , module sklearn.linear_model, $\alpha$ (regularization)={ $10^{-i}$ } $_{i=1}^5$ , { $5 \cdot 10^{-i}$ } $_{i=1}^5$
Logistic regression	<b>logreg</b>	Matlab	Function <b>mnrfit</b>
		Python	Function <b>LogisticRegression</b> , module sklearn.linear_model
Decision trees	<b>ctree</b> : classification tree	Matlab	Function <b>fitctree</b>
		Python	Function <b>DecisionTreeClassifier</b> , module sklearn.tree, criterion={Gini,entropy}, splitter={best,random}, max. features=3, 4, $I$ , $I/4$ , $I/2$ , $\sqrt{I}$ , $\log_2(I)$
		R	Function <b>ctree</b> , package party, max. depth=1..5, min. criterion={0.01, 0.5, 0.745, 0.99}

<sup>1</sup><https://github.com/concavegit/kfda>

<sup>2</sup><https://www.csie.ntu.edu.tw/~cjlin/libsvm>

	<b>rpart</b> : recursive partitioning	R	Function <b>rpart</b> , package <b>rpart</b>
Naive Bayes	<b>nb</b>	Matlab	Function <b>fitcnb</b>
		R	Function <b>NaiveBayes</b> , package <b>klaR</b>

The classifier performance is assessed by the Cohen’s kappa value (K), which measures the agreement between the true and predicted categories labels excluding the agreement by chance [22]. Other performance measures are the accuracy, sensitivity or recall, specificity, positive predictivity or precision, F1 and area under the receiver operating curve (AUC), see our reference [16] for a description of these measures.

3. Experimental setup and Results

3.1. Experimental setup

The information related to each patient is of two types:

- 1. Vector *clinical*, containing information related to patient life and its histopathology status before any treatment, composed by the following nine values: liver metastasis, pulmonary metastasis, sex (dicotomical variable), age, location of the tumour, T staging (0, 1, 2, 3 or 4), N staging (0, 1 or 2), M staging (0 or 1) and tumour differentiation (stages 1 to 4).
- 2. *Texture feature* vectors, with features extracted from each slice of the CT, in our case three slices of the tumour for each patient (56 patients multiplied by 3 cuts per patient).

The classifier performance is assessed using the leave-one-patient-out cross-validation approach. This methodology uses one patient (i.e., three cuts) to test the model and the remaining ones to train the model and to adjust its tunable hyper-parameters (see in table 1 the values of the tunable parameters of each model). All the inputs are pre-processed to have zero mean and standard deviation one. This process is repeated as many times as patients, each time using a different test patient. Finally, the performance is calculated comparing the label predicted by the classifier and the gold standard for determining KRAS mutation for each patient. In the case of texture feature vectors, we have an input vector for each cut of the patient’s tumor, and then a classifier output (or prediction) for each cut. The classifier prediction is selected by most voted among the three predictions, one for each cut.

3.2. Results

We developed experiments applying the 34 classifiers using as input: 1) the clinical vector; 2) the 27 texture feature vectors; and 3) the combinations of *clinical* vector and the 27 texture feature vectors. The texture feature vectors used are: eight Haralick vectors  $Hf_{dm}$ ,  $\{Hf_{dm}, d=1, 2, 3, 123, m=4, 5\}$ , four  $LBP_R$ ,  $\{LBP_R, R=1, 2, 3, 123\}$ , four  $LBP_s$ ,  $\{LBP_s, s=1, 2, 3, 123\}$ , vector DWT, six  $WCF_{dm}$ ,  $\{WCF_{dm}, d=1, 2, 3, m=4, 5\}$ , and four  $WDCF_{fm}$  vectors  $\{WDCF_{fm}, f=LL, All, m=4, 5\}$ . Overall, we performed  $34(1+27+27) = 1,870$  experiments.

**Table 2.** The list of top-10 best combination of a feature vector and classifier, which achieved the highest kappa and accuracy to predict the KRAS mutation.

Position	Kappa (%)	Accuracy (%)	Dataset	Classifier	Language
1	53.7	76.8	clinical	adaboost	Python
2	46.0	73.2	$Hf_{d123m4}$ +clinical	mlp	Python
3	46.0	73.2	$WDCF_{fm}$ (m=4, f=All)	rpart	R
4	46.0	73.2	$WDCF_{fm}$ (m=5, f=All)	rpart	R
5	45.7	73.2	$WCF_{d3m5}$ +clinical	ridge	Matlab
6	44.9	73.2	$Hf_{d3m4}$ +clinical	ridge	Matlab
7	42.9	71.4	clinical	mlp	Python
8	42.6	71.4	clinical	elm	Octave
9	42.6	71.4	$Hf_{d2m4}$ +clinical	lda	Octave



10	42.3	71.4	Hfd2m4 +clinical	logreg	Matlab
----	------	------	------------------	--------	--------

Table 2 shows the list of top-10 best combination of a feature vector and classifier to predict the KRAS mutation. The highest kappa value (53.7%) and accuracy (76.8%) was achieved by the the **adaboost** (adaptive boosting ensemble) classifier implemented in Python using the *clinical* vector. The best performance using only feature texture vectors (image information) was provided using the combination of wavelet and Haralick’s coefficients (feature vector WDCF<sub>fm</sub> with *f*=All bands and *m*=4), achieving a kappa=46.0% and accuracy=73.2%. The combination of clinical and imaging information did not exceed the results achieved by the clinical information alone.

**Table 3.** Confusion matrix to determine the KRAS mutation using as input the clinical information (vector clinical) and the imaging information (vector WDCF). Position 1 and 3 in table 2.

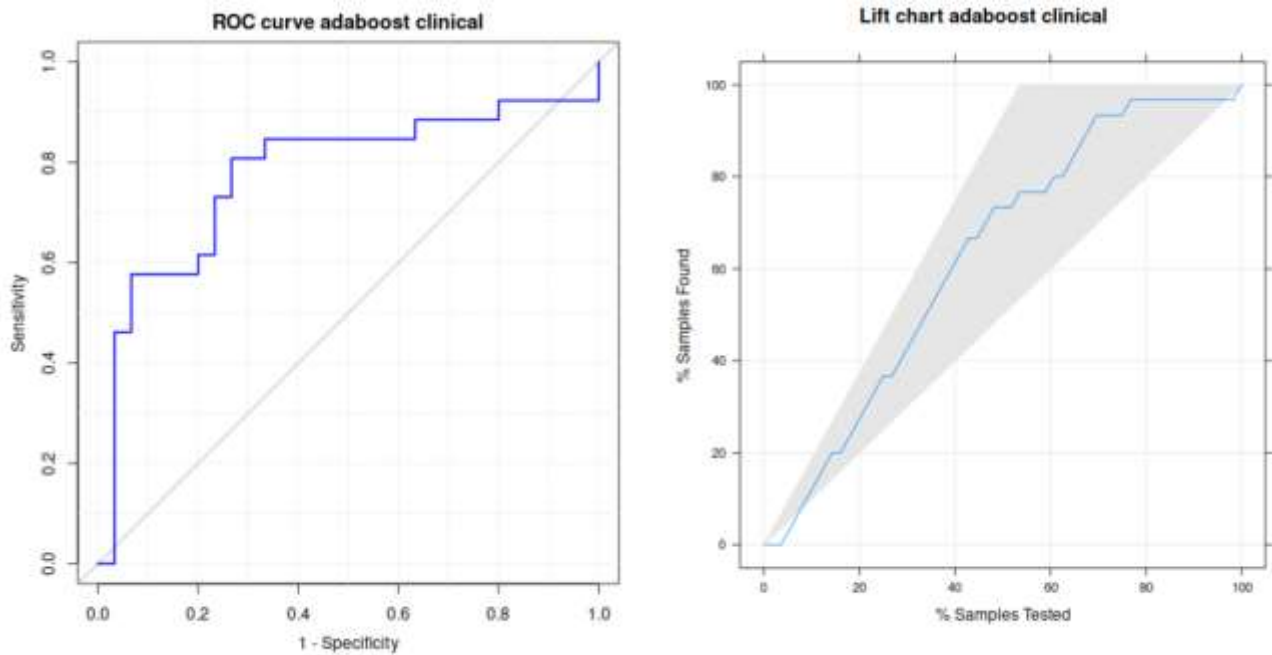
Dataset		Biopsy		
			KRAS +	KRAS -
Clinical information	<b>Computer</b>	KRAS+	<b>22 (39.3%)</b>	8 (14.3%)
kappa=53.7% acc=76.8%	(adaboost)	KRAS-	5 (8.9%)	<b>21 (37.5%)</b>
WDCF <sub>fm</sub> ( <i>f</i> =All)	<b>Computer</b>	KRAS+	<b>23 (41.1%)</b>	7 (12.5%)
kappa=46% acc=73.2%	(rpart)	KRAS-	8 (14.3%)	<b>18 (32.1%)</b>

Table 3 shows the confusion matrix for the best performance for clinical and imaging information. Although the difference between both confusion matrices is small, they lead to a large difference in kappa, 53.7% and 46% using clinical (up) and WDCF<sub>fm</sub> (down). However, the difference in accuracy (76.8% and 73.2%) is much smaller. In the best result, achieved by adaboost using the clinical vector (up), the terms outside the diagonal (5 and 8 false negatives and positives, respectively) are much smaller than terms in the diagonal (22 and 21 true positive and negatives, respectively).

**Table 4.** Performance metrics (in %) achieved by the best classifier (adaboost) and feature vector (clinical patient information).

Kappa	Accuracy	Sensitivity / Recall	Specificity	Precision / positive predictivity value (PPV)	F1	AUC
53.7	76.8	73.3	80.8	81.5	77.2	77.8

Other performance metrics for the best classification are reported in Table 4. Specifically, adaboost achieves a high sensitivity (73.3%), specificity (80.8%) and area under the receiver operating curve (ROC), that is (in %) 77.8%. The left panel of Figure 2 plots this curve, that is quite near to the upper left corner that identifies ideal classification. The right panel plots the lift curve, where the black line inside the gray shadowed area is also fairly near to the left border of this area identifying the ideal classification.



**Figure 2.** Graphical representation for the best configuration to predict KRAS mutation: classifier adaboost with the clinical vector as input. (a) ROC curve. (b) Lift chart.

In order to analyse the behaviour of different texture features families, Table 5 shows the best performance achieved by a vector of each descriptor family. The highest kappa (46%) and accuracy (73.2%) is achieved by the combination of Haralick coefficients and wavelets using all bands (WDCF<sub>fm</sub> vector with  $f=All$  and  $m=4$  or  $m=5$ ) using the rpart classifier (recursive partitioning decision tree), implemented in the R language. Indeed, four of 6 best results were achieved by classification trees (ctree and rpart). The other way to compute Haralick coefficients over wavelet decomposition (vectors WCF<sub>dm</sub>) achieved much lower performance (kappa=28.2%). The local binary patterns (LBP<sub>R</sub> and LBP<sub>s</sub> vectors) provided similar results (kappa=35.0% and 36.9% respectively), but also much lower than WDCF<sub>fm</sub> vector. The worst texture descriptor is the DWT vector (kappa=12% using diagonal linear discriminant analysis).

**Table 5.** Highest kappa (in %) achieved by each family of texture descriptors, with the best classifier and its implementation language.

Texture descriptor	Kappa(%)	Configuration	Classifier	Language
Hf <sub>dm</sub>	24.7	$d=123, m=5$	ctree	R
LPB <sub>R</sub>	35.0	$R=1$	ctree	Python
DWT	12.0	--	dlda	Matlab
LBP <sub>s</sub>	36.9	$s=2$	ridge	Matlab
WCF <sub>dm</sub>	28.2	$d=1$	rpart	R
WDCF <sub>fm</sub>	46.0	$f=All, m=4$	rpart	R

Table 6 shows the performance achieved using *clinical* and texture feature vectors concatenated as input to the classifier. The performance increased in almost all the texture families, but it is still lower than the performance achieved using only the *clinical* vector. The highest kappa is achieved by the combination of *clinical* and Hf<sub>dm</sub> vector (using  $d=123$  and  $m=4$ ) and the mlp (multi-layer perceptron) classifier implemented in Python. Nevertheless, all the combinations provided quite similar results (kappa value higher than 42%), except to DWT (kappa=34.7%) and WDCF<sub>fm</sub> (38.8%). It's a surprise that WDCF<sub>fm</sub> concatenated with *clinical* vector decreased its performance compared to WDCF<sub>fm</sub> alone (kappa=46% in Table 5 and 38.8% in Table 6).

**Table 6.** Highest kappa (in %) achieved concatenating the texture descriptor of each family with the clinical vector. .

Texture descriptor	Kappa(%)	Configuration	Classifier	Language
Hf <sub>dm</sub>	46.0	d=123, m=4	mlp	Python
LBB <sub>R</sub>	42.0	R=3	adaboost	Python
DWT	34.7	--	gbm	Python
LBP <sub>s</sub>	42.0	s=1	neuralnet	R
	42.0	s=3	adaboost	Python
WCF <sub>dm</sub>	45.7	d=3, m=5	mlp	Python
WDCF <sub>fm</sub>	38.8	f=LL, m=4	sgd	Python

4. Discussion

This study demonstrates that it is possible to predict KRAS mutation in CRC patients using a CT-based radiomics features. There is a relationship between the quantitative features obtained from the images and the KRAS oncogene mutation. The value of Cohen's Kappa coefficient shows that the relationship is not simply justified by chance. Compared to our previous investigations [19], we have increased the number of patients and tried a larger and more diverse collection of classifiers, including also patient clinical features. In the current work, the results achieved using only clinical information, only radiomics information and combined (clinical and radiomics) were similar, but slightly better using only clinical information. This demonstrates that clinical variables also provide useful information that can be unified with radiomic data to create a more effective combined model. The implementation of clinical data into radiomic studies is a growing field in recent years. Studies that combine clinical and radiomics features are becoming increasingly common. These studies often show improved results with clinical-radiomic association. For instance, Yuntai Cao et al. [23] developed a model that combines radiomic parameters with other clinical parameters such as age, CEA (carcinoembryonic antigen) level and clinical stage for the prediction of KRAS status. They achieved results similar than ours. His AUC, sensitivity and specificity was higher with the combined model (0.772, 0.792 and 0.646 respectively). Our results, together with those published in the literature, reflect the need for further research into the development of a combined model and the search for the best clinical-radiomic combination.

A recent revision published by our research group shows that studying the KRAS status is an expanding field. There are numerous studies published on this topic between 2018 and 2022 [14]. In December 2022, Jia et al [24] performed the first meta-analysis on this topic which includes 29 articles published between February 2014 and March 2022. Approximately 60% were recent (2020 and 2021). This review reflects the multiple imaging modalities to which KRAS status analysis is applicable (CT, PET, MRI). MRI was the most widely used, but the meta-analysis concluding that the diagnostic performance of CT is higher. Only one prospective design was included. The main criticisms of meta-analysis studies can be summarized in two aspects: low quality and heterogeneity. The sample size and segmentation methods are sources of variability between studies. The conclusion is that radiomics is at an early stage in terms of determining KRAS status, therefore prospective multicenter studies with standardized protocols are needed to achieve effective implementation in routine clinical practice.

Comparing with other similar studies, several aspects of our research should be highlighted. All the studies compared are retrospective. The sample size of our study is similar to other similar published studies, like Taguchi et al. [25], who created a model to predict KRAS mutation in CRC. They obtained an AUC between 0.4 and 0.7 with 40 patients. The slice thickness varies between 1 and 5 mm depending on the study. KRAS is the oncogene analyzed in all the studies, but Yang et al [26] analyzes as well NRAS and BRAF mutations. They obtained an AUC, sensitivity and specificity of 0.869, 0.757 and 0.833. Yu Li et

al. also seeks to detect perineural invasion. They obtained an AUC of 7.793 and 0.862 in the prediction of perineural invasion and KRAS mutation [27].

Anatomopathological analysis will remain the gold standard for mutational analysis. However, it has limitations that could be solved if complemented by radiomic analysis. Radiomics based on CT images would cover the entire tumour area and possible metastatic sites, thus avoiding the false negatives associated with analyzing a single tumour fragment [28]. There is also a percentage of patients with primary resistance to anti-EGFR monoclonal antibodies. In addition, almost all of those who initially respond to these therapies will eventually become refractory to treatment [29]. Therefore, serial radiomic CT scans throughout the course of the disease would offer the possibility of detecting new mutations in KRAS that cause this resistance.

The limitations of our study do not differ from those mentioned by other authors. Firstly, we started from a small sample size obtained retrospectively from the records of a single center. Secondly, despite having an advanced electronic medical record system, it is difficult to filter which patients could meet the inclusion criteria for the study, as there are no databases of patients diagnosed with colorectal cancer in our autonomous community. This could lead to patient selection bias and hinder the applicability of radiomics in the future. As regards technical parameters, over the years the reconstruction of the images has evolved. The first slices compiled for this study were 5 mm and are now less than 2.5 mm. The trend is to use increasingly thinner slices, as this is one of the parameters that provides the greatest variability in radiomic studies. Finally, the segmentation is manual, which is associated with a high time consumption in the delimitation of the regions of interest and high level of subjectivity.

Lastly, we should consider extending mutational analysis to other genes such as BRAF, NRAS, mismatch repair genes and even to other sites such as metastases. This approach would be more integrative and would facilitate the use of radiomics throughout the entire period of the disease, from diagnosis to the evolution of metastases.

## 5. Conclusions

CT-based radiomics can predict the KRAS status. Specifically, the recursive partitioning classification trees trained on texture features extracted from the CT images (Haralick and Wavelet coefficients) achieve Cohen kappa and accuracy of 46% and 73.2%. These results prove the correlation between texture patterns and KRAS mutational status. The patient clinical parameters (including liver and pulmonary metastasis, location of the tumour, N and M staging, and tumour differentiation) further improved the performance of the radiomics model up to a Cohen kappa and accuracy of 53.7% and 76.8%, sensitivity and specificity of 73.3% and 80.8%, and area under ROC of 77.8% achieved by the ada-boost ensemble classifier. This clinical information should be also taken into account for the application of radiomics in daily clinical practice. Radiomics is not intended to replace current diagnostic methods such as biopsy and pathological analysis, but rather to complement them by analyzing the entire area of the primary tumour from the time of diagnosis and throughout the course of the disease.

**Supplementary Materials:** The following supporting information can be downloaded at: Preprints.org, Figure S1: title; Table S1: title; Video S1: title.

**Author Contributions:** For research articles with several authors, a short paragraph specifying their individual contributions must be provided. The following statements should be used “Conceptualization, J.P.A., R.A.M. and M.S.B.; methodology, E.C., M.F.D. and V.G.C.; software, E.C., M.F.D. and V.G.C.; validation, E.C., M.F.D., V.G.C., S.B.G., R.G.F., M.S.B.; formal analysis, J.P.A., S.B.G. and R.G.F.; investigation, J.P.A., E.C., R.A.M., M.F.D., V.G.C.; resources, E.C., M.F.D., V.G.C.; data curation, E.C., M.F.D.; writing—original draft preparation, J.P.A., R.A.M.; writing—review and editing, E.C. and S.B.G.; visualization, E.H.Z., R.G.F., J.R.A.L. and M.S.B.; supervision, E.G., E.H.Z., S.B.G., J.R.A.L. and M.S.B. All authors have read and agreed to the published version of the manuscript.”

**Funding:** This research received no external funding.

**Institutional Review Board Statement:** The study was conducted in accordance with the Declaration of Helsinki, and approved by the Ethics Committee of Santiago-Lugo (protocol code 2019/356, 22/10/2019).

**Informed Consent Statement:** Informed consent was obtained from all subjects involved in the study.

**Data Availability Statement:** We encourage all authors of articles published in MDPI journals to share their research data. In this section, please provide details regarding where data supporting reported results can be found, including links to publicly archived datasets analyzed or generated during the study. Where no new data were created, or where data is unavailable due to privacy or ethical restrictions, a statement is still required. Suggested Data Availability Statements are available in section "MDPI Research Data Policies" at <https://www.mdpi.com/ethics>.

**Acknowledgments:** This work has received financial support from Xunta de Galicia (ED431G-2019/04) and the European Regional Development Fund (ERDF), which acknowledges the CiTIUS - Centro Singular de Investigación en Tecnoloxías Intelixentes da Universidade de Santiago de Compostela as a Research Center of the Galician University System.

**Conflicts of Interest:** The authors declare no conflict of interest.

## References

1. Silva M, Brunner V, Tschurtschenthaler M. Microbiota and Colorectal Cancer: From Gut to Bedside. *Front Pharmacol*. 2021 Sep 30;12:760280. doi: 10.3389/fphar.2021.760280. PMID: 34658896; PMCID: PMC8514721.
2. Hanahan D, Weinberg RA. Hallmarks of cancer: the next generation. *Cell*. 2011 Mar 4;144(5):646-74. doi: 10.1016/j.cell.2011.02.013. PMID: 21376230.
3. O'Keefe SJ. Diet, microorganisms and their metabolites, and colon cancer. *Nat Rev Gastroenterol Hepatol*. 2016 Dec;13(12):691-706. doi: 10.1038/nrgastro.2016.165. Epub 2016 Nov 16. PMID: 27848961; PMCID: PMC6312102.
4. Nosh K, Sukawa Y, Adachi Y, Ito M, Mitsuhashi K, Kurihara H, Kanno S, Yamamoto I, Ishigami K, Igarashi H, Maruyama R, Imai K, Yamamoto H, Shinomura Y. Association of *Fusobacterium nucleatum* with immunity and molecular alterations in colorectal cancer. *World J Gastroenterol*. 2016 Jan 14;22(2):557-66. doi: 10.3748/wjg.v22.i2.557. PMID: 26811607; PMCID: PMC4716059.
5. Fearon ER, Vogelstein B. A genetic model for colorectal tumorigenesis. *Cell*. 1990 Jun 1;61(5):759-67. doi: 10.1016/0092-8674(90)90186-i. PMID: 2188735.
6. Vergara, Édgar, Alvis, N. y Suárez, A. 2019. ¿Existen ventajas clínicas al evaluar el estado de los genes KRAS, NRAS, BRAF, PIK3CA, PTEN y HER2 en pacientes con cáncer colorrectal?. *Revista Colombiana de Cirugía*. 32, 1 (jul. 2019), 45–55. DOI:<https://doi.org/10.30944/20117582.7>.
7. Currais P, Rosa I, Claro I. Colorectal cancer carcinogenesis: From bench to bedside. *World J Gastrointest Oncol*. 2022 Mar 15;14(3):654-663. doi: 10.4251/wjgo.v14.i3.654. PMID: 35321283; PMCID: PMC8919024.
8. Afrăsănie VA, Marinca MV, Alexa-Stratulat T, Gafton B, Păduraru M, Adavidoaiei AM, Miron L, Rusu C. KRAS, NRAS, BRAF, HER2 and microsatellite instability in metastatic colorectal cancer - practical implications for the clinician. *Radiol Oncol*. 2019 Sep 24;53(3):265-274. doi: 10.2478/raon-2019-0033. PMID: 31553708; PMCID: PMC6765160.
9. Garcia-Carbonero N, Martinez-Useros J, Li W, Orta A, Perez N, Carames C, Hernandez T, Moreno I, Serrano G, Garcia-Foncillas J. KRAS and BRAF Mutations as Prognostic and Predictive Biomarkers for Standard Chemotherapy Response in Metastatic Colorectal Cancer: A Single Institutional Study. *Cells*. 2020 Jan 15;9(1):219. doi: 10.3390/cells9010219. PMID: 31952366; PMCID: PMC7016634.
10. Zhu G, Pei L, Xia H, Tang Q, Bi F. Role of oncogenic KRAS in the prognosis, diagnosis and treatment of colorectal cancer. *Mol Cancer*. 2021 Nov 6;20(1):143. doi: 10.1186/s12943-021-01441-4. PMID: 34742312; PMCID: PMC8571891.
11. Schirripa M, Nappo F, Cremolini C, Salvatore L, Rossini D, Bensi M, Businello G, Pietrantonio F, Randon G, Fucà G, Boccaccino A, Bergamo F, Lonardi S, Dei Tos AP, Fassan M, Loupakakis F. KRAS G12C Metastatic Colorectal Cancer: Specific Features of a New Emerging Target Population. *Clin Colorectal Cancer*. 2020 Sep;19(3):219-225. doi: 10.1016/j.clcc.2020.04.009. Epub 2020 May 12. PMID: 32605718.
12. Limkin EJ, Sun R, Dercle L, Zacharaki EI, Robert C, Reuzé S, Schernberg A, Paragios N, Deutsch E, Féré C. Promises and challenges for the implementation of computational medical imaging (radiomics) in oncology. *Ann Oncol*. 2017 Jun 1;28(6):1191-1206. doi: 10.1093/annonc/mdx034. PMID: 28168275.
13. Gillies RJ, Kinahan PE, Hricak H. Radiomics: Images Are More than Pictures, They Are Data. *Radiology*. 2016 Feb;278(2):563-77. doi: 10.1148/radiol.2015151169. Epub 2015 Nov 18. PMID: 26579733; PMCID: PMC4734157.
14. Porto-Álvarez, J.; Barnes, G.T.; Villanueva, A.; García-Figueiras, R.; Baleato-González, S.; Huelga Zapico, E.; Souto-Bayarri, M. Digital Medical X-ray Imaging, CAD in Lung Cancer and Radiomics in Colorectal Cancer: Past, Present and Future. *Appl. Sci*. 2023, 13, 2218. <https://doi.org/10.3390/app13042218>
15. Sonka, M. , Václav, H. and Boyle, R. Image processing, analysis and machine vision, Thomson, 2008. <https://dl.acm.org/doi/abs/10.5555/1537182>



16. Cernadas, E., Fernández-Delgado, M., González-Rufino, E. and Carrión, P. Influence of normalization and color space to color texture classification. *Pattern Recognition*. 2017 (61):120-138. Doi: 10.1016/j.patcog.2016.07.002.
17. Haralick, R.M.; Shanmugam, K.; Dinstein, I. Textural features for image classification. *IEEE Trans. Syst. Man. Cybern.* 1973, 3, 610–621.
18. Manuel Fernández-Delgado, Eva Cernadas, Senén Barro, and Dinani Amorim. 2014. Do we need hundreds of classifiers to solve real world classification problems? *J. Mach. Learn. Res.* 15, 1 (January 2014), 3133–3181. <https://dl.acm.org/doi/10.5555/2627435.2697065>
19. González-Castro, V.; Cernadas, E.; Huelga, E.; Fernández-Delgado, M.; Porto, J.; Antunez, J.R.; Souto-Bayarri, M. CT Radiomics in Colorectal Cancer: Detection of KRAS Mutation Using Texture Analysis and Machine Learning. *Appl. Sci.* 2020, 10, 6214. <https://doi.org/10.3390/app10186214>
20. T. Ojala, M. Pietikainen and T. Maenpaa, "Multiresolution gray-scale and rotation invariant texture classification with local binary patterns," in *IEEE Transactions on Pattern Analysis and Machine Intelligence*, vol. 24, no. 7, pp. 971-987, July 2002, doi: 10.1109/TPAMI.2002.1017623.
21. González-Rufino, E., Carrión, P., Cernadas, E., Fernández-Delgado, M., Domínguez-Petit, R. Exhaustive comparison of colour texture features and classification methods to discriminate cells categories in histological images of fish ovary. *Pattern Recognition*. 2013 (46): 2391-2407. Doi: 10.1016/j.patcog.2013.02.009.
22. McHugh ML. Interrater reliability: the kappa statistic. *Biochem Med (Zagreb)*. 2012;22(3):276-82. PMID: 23092060; PMCID: PMC3900052.
23. Cao Y, Zhang J, Huang L, Zhao Z, Zhang G, Li H, et al. Development and Validation of Radiomics Signatures to Predict KRAS Mutation Status Based on Triphasic Enhanced Computed Tomography in Patients with Colorectal Cancer. *Research Square [Internet]* 2022 [Feb 2023]; Available on: <http://dx.doi.org/10.21203/rs.3.rs-1261428/v1>
24. Jia L-L, Zhao J-X, Zhao L-P, Tian J-H, Huang G. Current status and quality of radiomic studies for predicting KRAS mutations in colorectal cancer patients: A systematic review and meta-analysis. *Eur J Radiol [Internet]*. 2023 [Feb 2023];158:110640. Available on: <https://doi.org/10.1016/j.ejrad.2022.110640>
25. Taguchi N, Oda S, Yokota Y, Yamamura S, Imuta M, Tsuchigame T, et al. CT texture analysis for the prediction of KRAS mutation status in colorectal cancer via a machine learning approach. *Eur J Radiol [Internet]*. 2019 [Dec 2022];118:38-43. Available on: <https://doi.org/10.1016/j.ejrad.2019.06.028>
26. Yang, L., Dong, D., Fang, M. et al. Can CT-based radiomics signature predict KRAS/NRAS/BRAF mutations in colorectal cancer?. *Eur Radiol* 28, 2058–2067 (2018). <https://doi.org/10.1007/s00330-017-5146-8>
27. Li Y, Eresen A, Shanguan J, Yang J, Benson AB 3rd, Yaghmai V, Zhang Z. Preoperative prediction of perineural invasion and KRAS mutation in colon cancer using machine learning. *J Cancer Res Clin Oncol*. 2020 Dec;146(12):3165-3174. doi: 10.1007/s00432-020-03354-z. Epub 2020 Aug 10. PMID: 32779023.
28. Cao J, Wang GR, Wang ZW, Jin ZY. CT Texture Analysis: A Potential Biomarker for Evaluating KRAS Mutational Status in Colorectal Cancer. *Chin Med Sci J*. 2020 Dec 31;35(4):306-314. doi: 10.24920/003770. PMID: 33413746.
29. Leto SM, Trusolino L. Primary and acquired resistance to EGFR-targeted therapies in colorectal cancer: impact on future treatment strategies. *J Mol Med (Berl)*. 2014 Jul;92(7):709-22. doi: 10.1007/s00109-014-1161-2. Epub 2014 May 10. PMID: 24811491; PMCID: PMC4055851